IOP Publishing Journal of Physics: Condensed Matter

J. Phys.: Condens. Matter **22** (2010) 495101 (15pp) doi:10.1088/0953-8984/22/49/495101

Utility of continuum diffusion models for analyzing mobile-ion immittance data: electrode polarization, bulk, and generation–recombination effects

J Ross Macdonald

Department of Physics and Astronomy, University of North Carolina, Chapel Hill, NC 27599-3255, USA

E-mail: macd@email.unc.edu

Received 10 August 2010, in final form 18 October 2010
Published 16 November 2010
Online at stacks.iop.org/JPhysCM/22/495101

Abstract

Consequences of the well-known Poisson–Nernst–Planck (PNP) continuum equations of charge motion in liquids or solids for ordinary or anomalous diffusion are investigated for an electrochemical cell with completely blocking electrodes. Previous work is summarized and much of it is shown to be independent of earlier published results and incomplete, with little comparison made between ordinary and anomalous diffusion. Such comparison is provided here and also includes variation of the mobility ratio of the mobilities of positive and negative charges from equality to charge of only one sign mobile. New generation–recombination effects are demonstrated for a range of mobility ratios, with particular attention given to those present for the case of charge of only one sign mobile. No previous analyses of experimental data with PNP models using complex-least-squares fitting have been published. Here such a model is found to fit frequency response data well for a hydrogel and to lead to estimates of physically meaningful parameters such as the diffusion constant and ionic concentration. PNP analysis of a synthetic data set derived from experimental results for liquid electrolytes refutes claims made in the original publication dealing with it, but verifies and extends an interesting analysis equation proposed there. PNP fitting of data for solids, including ones showing colossal low-frequency-limiting dielectric constants, suggests that they may often be well described as arising from simple diffuse-charge double-layer effects, and that continuum microscopic models such as the PNP, in series with a conducting Debye response model, may be sufficient for fitting well an appreciable amount of data involving ion hopping and trapping behavior.

1. Introduction

In the present work the frequency response and usefulness of effective-medium models derived from the microscopic Poisson–Nernst–Planck continuum equations, with either conventional (PNP) or anomalous diffusion (PNPA), are considered, particularly for mobile ions completely or nearly blocked at non-parent-ion metallic electrodes. A parameter ψ ($0 < \psi \leqslant 1$) is unity for the PNP model and less than one for the PNPA. In these analyses, Poisson's equation must be satisfied throughout the ion-containing material. Situations with ions of both signs equally mobile are first considered. This is the two-mobile case, particularly appropriate for liquids. In addition, results are presented for ions of only one sign mobile: the one-mobile case, usually most appropriate for solids, a situation where generation–recombination (GR) of charge may play an important role.

Although much theoretical work in this area has been published since 1953 [1–10], only a few calculated full-model immittance response plots have appeared, for example, those in [6], which included only complex-plane responses, and the recent results of [10] which included one-mobile GR effects. Further, thus far it appears that only a simplified PNP model has been used for data fitting [8]. More details

about these and other relevant analyses are included in the appendix, section A.3. Also pertinent to the present area is the comprehensive 2004 review paper of Bazant *et al* on diffuse-charge dynamics [11].

The full PNP analysis of [4] includes several types of possible generation–recombination processes, and its results have been included since about 1993 as a fitting choice in the LEVM complex-nonlinear-least-squares (CNLS) computer program [12][1], but, until recently [10], other analyses ignored such effects. Of particular interest is the simplest GR situation where neutral entities may dissociate into positive and negative mobile changes with possibly different valences. This situation with unity valence numbers is that considered in [10], a treatment that followed the approach described in [4] but solved the relevant equations independently. Its results and comparable ones calculated using LEVM from the formulas of [4] are discussed in section 2.2.

It is particularly significant that although the continuum PNP model shows dispersion arising from the diffusion of mobile ions, and thus may be considered a conductive-system model, in its simplest form it leads to complete blocking at the electrodes and thus to a low-frequency-limiting value of zero for the real part of the conductivity [2]. Its close relation to dielectric-system pure dielectric response of Debye character is discussed in appendix A.3. Note that the PNP model is an effective-medium microscopic one that includes no explicit treatment of such processes as hopping, trapping, and lattices, common in more detailed theories of charge motion in condensed materials [13–17]. Thus, it is natural and important to ask how well it can represent experimental data for a range of different materials, data that have been fitted in the past by other more detailed macroscopic and microscopic models.

The value of such continuum models for fitting materials with and without an additional conductive-system Debye or Davidson–Cole [18] response model in series (see appendix A.2) is illustrated here, while work in progress deals with such analysis of data for solid polymers, fast-ion solid conductors, and CKN [16]. The utility of PNP and PNPA continuum models for fitting and interpreting such data will be compared with those of traditional fitting models, particularly hopping ones derived from Kohlrausch stretched-exponential temporal response [14, 15, 19–24].

Although the individual bulk models usually require three or four parameters to define them fully, it is generally found that the goodness-of-fit of experimental data is much improved by the addition of one or more additional circuit elements, such as resistors or capacitors in series or parallel with the bulk model. For example, a series Debye conductive-system relaxation model, involving a resistance and capacitance in parallel, will be designated by Deb, while a parallel dielectric Debye model, involving a resistance and capacitance in series, will be referred to as DebD.

[1] The newest WINDOWS version, LEVMW, of the comprehensive LEVM fitting and inversion program may be downloaded at no cost by accessing http://jrossmacdonald.com. It includes an extensive manual and executable and full source code. More information about LEVM is provided at this internet address. All of the Ross Macdonald papers cited herein are available in PDF format for downloading from this address.

Composite model names apply here for the original experimental data level but actual fitting will be mostly carried out for data in specific form. Thus, for example, a capacitance, C, is designated ε (the relative dielectric permittivity or dielectric constant) after transformation to specific form. See appendix A.1. Here the · symbol denotes a series connection and its absence a parallel one. Thus, the designation GPNP · Deb indicates a constant conductance G (specific name $\sigma' \equiv \sigma_P$) in parallel with a bulk microscopic PNP model, and the combination in series with a resistivity-level Debye model.

Section 2.1 illustrates PNP and PNPA frequency responses and shows significant differences between them for full-dissociation situations, while GR behavior [4, 10, 25, 26] is discussed in section 2.2. Section 3 illustrates fitting of hydrogel data [27] with various composite models, including PNP and PNPA bulk ones [4, 25]. Section 4 considers synthetic data derived from liquid-electrolyte frequency response measurements [28] and shows how it may be well analyzed using composite PNP models. Finally, section 5 discusses some possible PNP/PNPA model limitations.

The appendix summarizes provenance and background information about the various fitting models used here, with special emphasis on the PNP–PNPA ones. The present PNPA response model, which includes the PNP and is described in detail in appendix A.3, has not been previously used for CNLS fitting of experimental data, even though it is implicitly present in the 1953 work of [1].

2. Comparison of some PNP and PNPA model frequency responses

2.1. PNP and PNPA responses with full dissociation

Although many PNP model epsilon-level complex-plane synthetic data plots have been presented in [6], including generation–recombination effects and different mobilities and valences for positive and negative mobile charge situations, all under completely blocking conditions, detailed PNP and PNPA real and imaginary frequency immittance responses have not been shown. Therefore, we show here some PNP responses and compare them with anomalous diffusion PNPA ones, and both models, described in appendix A.3, are used for LEVM fitting and analysis in subsequent sections. These two models are employed for fitting in the present section, however, only in simplified form where charges have equal valences, full dissociation, and with either equal mobilities for positive and negative charges or only one type mobile [2, 4, 10, 25]. However, the Circuit-H LEVM program, some of whose results are discussed in section 2.2, involves a general PNPA model, including partial or complete blocking of charges at the electrodes, GR, and any ratio of positive and negative charge mobilities.

Figure 1 shows some dielectric-level PNP and PNPA complex-plane responses with the figure 1(a) $\varepsilon'(0)$ quantities normalized to unity for easy comparison of the shapes of the results. Note that the PNPA model reduces to the PNP one when $\psi = 1$, and that the PNP/PNPA interface response,

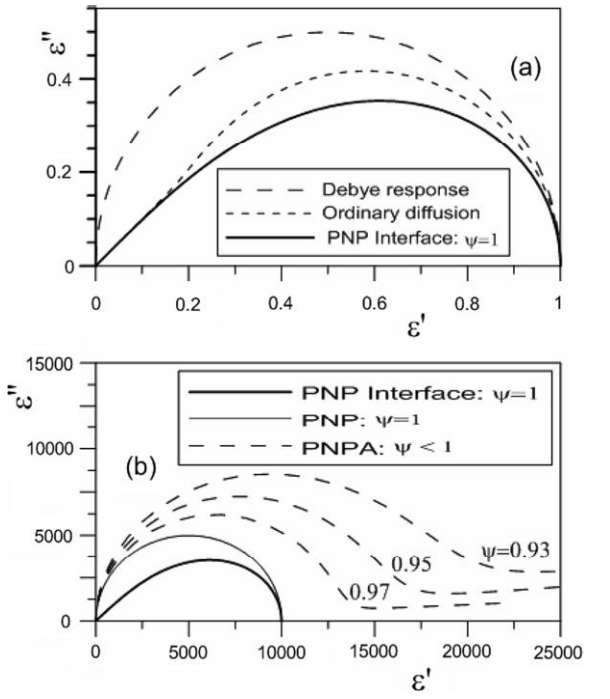

Figure 1. (a) Complex-plane plots comparing Debye response, ordinary infinite-length Warburg diffusion, and the PNP interface normalized responses defined in appendix (A.3). (b) The un-normalized PNP complex-plane interface response is shown along with PNPA responses for some $\psi \leqslant 1$ values.

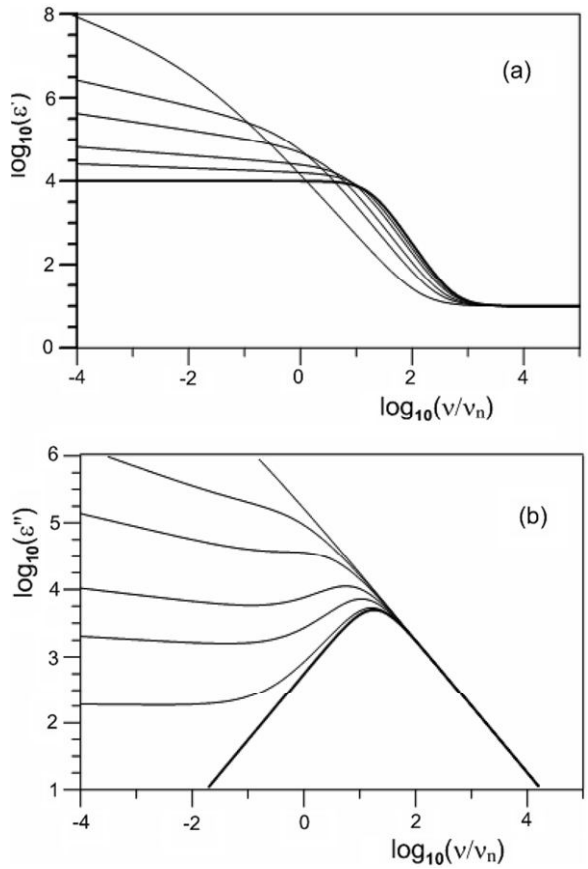

Figure 2. Log–log plots of $\varepsilon(\nu)$ PNPA response for $\rho_\infty = 10^7\ \Omega$ cm, $\varepsilon_\infty = 10$, and $M = 10^3$ with for various ψ values. (a) Top-down ψ values are: 0.5, 0.7, 0.8, 0.9, 0.95, and 1. (b) Top-down ψ values are: 0.5, 0.7, 0.8, 0.9, 0.95, 0.99, and 1. Here and elsewhere the frequency $\nu_n = 1$ Hz is used for normalization since logarithmic arguments must be dimensionless.

defined in equation (A.11), is appreciably different from that of ordinary finite-length Warburg diffusion which does not require satisfaction of the Poisson equation. Further, as shown in figure 1(b), full anomalous PNPA response can differ appreciably from that of its PNP limit. Here the nomenclature 'Interface' designates the diffusional part of the full bulk response, where the latter is defined in equation (A.10).

Figures 2 and 3 illustrate the effects of various ψ values for $\varepsilon(\nu)$ and $\sigma(\nu)$ real and imaginary responses and involve the parameter values $\rho_\infty \equiv 1/\sigma_\infty = 10^7\ \Omega$ cm, $\tau_P = 8.854\,19 \times 10^{-6}$ s, $M \equiv L/2L_D = 10^3$, $\varepsilon_\infty = 10$, and $\psi \leqslant 1$. Here L_D is the Debye screening length. For figure 2(a) and $\psi = 1$, $\varepsilon'(0) \equiv \varepsilon_0 = M\ \mathrm{ctnh}(M)\varepsilon_\infty$, a large value here. The quantity L is the separation of plane-parallel electrodes. For two-mobile situations L_D may be expressed as $[\varepsilon_V \varepsilon_\infty k_B T/\{e^2(z_n^2 n_0 + z_p^2 p_0)\}]^{1/2}$, where k_B is Boltzmann's constant and e is the magnitude of the electron charge. When only one of the charge concentrations, n_0 or p_0, is mobile, only that one appears in L_D [4, 25]. When $n_0 = p_0$, as in the uni-univalent intrinsic generation–recombination situation discussed later, then $L_{D1} = \sqrt{2}L_{D2}$.

In recent years, much attention has been devoted to giant, colossal low-frequency relative dielectric constants, ones often even greater than 10^5 [29–31]. It has led to the conclusion that such behavior is extrinsic and is associated with interface and/or electrode polarization, as opposed to intrinsic ε_∞ response. Results for both ceramic and single-crystal materials have been tentatively ascribed to thin exhaustion layers at electrodes, ones possibly associated with Schottky diodes involving electronic conduction.

Alternatively, the formation of PNP ionic diffuse double layers abutting electrodes may explain some of the colossal dielectric constants observed so far. When charges of both signs are mobile, the diffuse double layers at the electrodes involve charge accumulation layers. It is significant that, in the absence of GR effects and for conditions where all parameter values are the same except for the mobility ratio, the PNP ε_0 value for the equal-mobility case is the $\sqrt{2}$ times that for the one-mobile situation. In addition, the time constant formed by the product of the low-frequency resistance and capacitance is twice as large for the one-mobile case as that of the two-mobile one.

Further, it is particularly noteworthy that $\varepsilon(\nu)$ and $\sigma(\nu)$ responses very similar to those of figures 2 and 3 appear in [29–31]. In addition, the remarkable experimental decrease of ε_0 to ε_∞ as the temperature approaches zero [29–31] is well explained for the one-mobile PNPA model, where $L_{D1} \propto [T/n_0]^{1/2}$. When n_0, the mobile charge concentration, is thermally activated and thus decreases faster than does T, then $M\mathrm{ctnh}(M) \to 1$ as $L_D \to \infty$.

Note that for $\psi = 1$ the low-frequency slope of $\sigma'(\nu)$ on the log–log plot (called just 'slope' hereafter) is two, while for $\psi < 1$ the decrease in $\sigma'(\nu)$ from its σ_∞ high-frequency

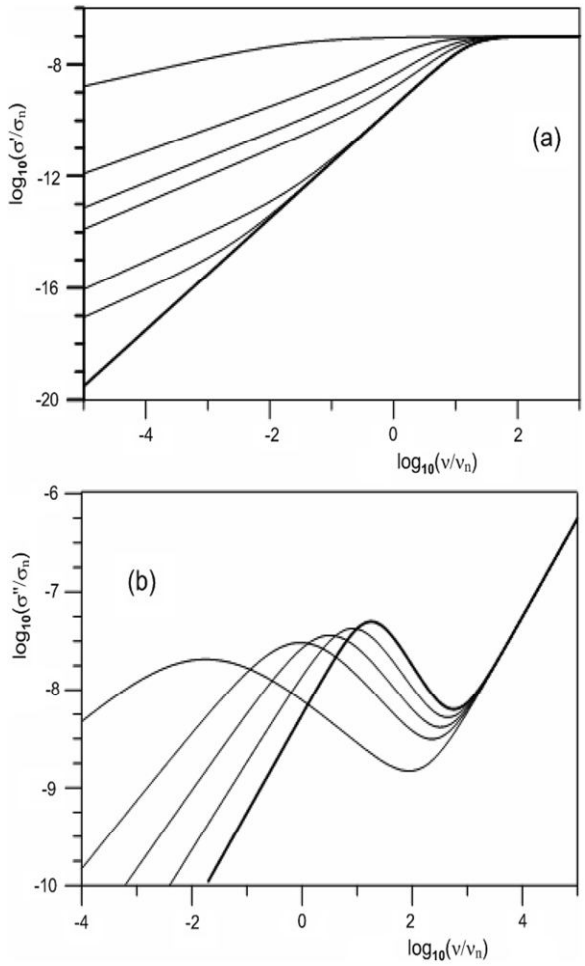

Figure 3. Log–log plots of $\sigma(\nu)$ PNPA response for the same parameter values as in figure 2 with various ψ values. (a) Top-down ψ values are: 0.5, 0.8, 0.9, 0.95, 0.99, 0.9999, and 1. (b) Left-to-right ψ values are: 0.5, 0.7, 0.8, 0.9, and 1. Here and elsewhere $\sigma_n = 1$ s cm^{-1}.

plateau value starts with a slope of two but soon approaches that of the ψ value. The corresponding $\varepsilon''(\nu)$, as shown in figure 2(b), approaches a low-frequency slope of $1 - \psi$, the often observed nearly constant loss (NCL) behavior for ψ near unity.

There are two types of frequency response not modeled by the usual equal-mobility PNP model. First, one often observes an increase from the $\rho'(\nu)$ plateau response of $\rho_0 = 1/\sigma_\infty$ at frequencies below that region of constant low-frequency response. Although such an increase appears for the PNPA model but not the PNP one, it is often insufficient in size to model experimental response in this region adequately. On the other hand, a very small parallel conductivity, σ_P, leading to a high zero-frequency resistivity, can lead to such response as illustrated later, as can GR effects.

Second, at high frequencies, particularly for solid electrolytes, one often sees a progressive increase in $\sigma'(\nu)$ at high frequencies above the σ_∞ plateau. This effect has been usually modeled by the series addition of a Deb, DC0, or constant-phase SC model. In contrast, low-frequency rises in $\rho'(\nu)$ above a ρ_0 plateau may originate from mobility differences between positive and negative ions and from GR effects, as briefly discussed in section 2.2.

2.2. PNP and PNPA model responses with generation–recombination

The general PNP model considered here involves the generation and recombination of mobile charges from neutral entities of concentration N_0 that may dissociate into positive and negative charges [1, 2, 4, 25]. A complete-blocking, two-mobile LEVM fitting program including GR effects and arbitrary mobilities and valences is based on equation (32) in [4]. As a check of it, a separate and simpler program where the mobility of charge of one sign equals zero, involving equation (40), is also available there and in the earlier [25], and it is used herein where appropriate. Here, as in the recent GR response work of [10], unity valence numbers are assumed and the valence-number ratio, Π_Z, is unity.

The work of [10] started from the basic PNP GR equations of [1, 4] and, rather than using the results in those works to generate response curves, the authors derived independent expressions for the impedance in the completely blocking case. Because their parameters and notation are substantially different from those used in [4] and in earlier related work of the present author [2, 25], it is difficult to verify that their impedance expressions are identical to those in the earlier work. Therefore, numerical one-mobile data sets generated by their program have been fitted, using LEVM, to [4, 25] expressions to test for agreement, a useful check on the validity of all these approaches.

Because the analysis and results of [10] deal with impedance rather than with data in specific form, that will also be the case here to allow easy comparison of results. Although an expression for the impedance of a two-mobile material is derived in [10], unlike that considered here it applies only for charges of equal mobilities, and a separate analysis is presented for the one-mobile case. Only for this case are GR immittance frequency response plots included in [10]. Its impedance-level results agree with earlier ones [2, 4] in the full-dissociation case where the general form of the response function is the same for equal-mobility and one-mobile cases.

In the one-mobile case, the authors of [10] demonstrate the appearance of a 'new' (second) plateau at lowest frequencies in the real part of the impedance. Because the earlier GR work of [25] was not cited in their work, they were unaware that there it was shown that not only this low-frequency plateau, as well as another one associated with electrode reactions could appear, making a total of three possible plateaus. Also even in the complete-blocking situation a third plateau may arise for unequal but not infinite mobility ratios, as discussed later. Finally, an earlier version of the present work was shared with Barbero, an author of [10], and he and a co-author have recently submitted for publication a manuscript dealing particularly with the one-mobile plateau situation [26] and, as discussed later, they have thereby independently verified some of the GR results in the present section.

The dissociable entities considered here may be of intrinsic, donor, or acceptor character with a bulk density N_0,

here expressed in cm^{-3} units. Generation and bimolecular recombination parameters are denoted by k_g (units s^{-1}) and k_r (units $cm^3\ s^{-1}$), respectively, and often appear in the quotient $k_{gr} \equiv k_g/k_r$. For simplicity, denote the logarithm of this important quantity, expressed in dimensionless form, as *KDL*, a convenient measure of charge dissociation. Here, as in [10], we set k_g to 1 s^{-1}; therefore as k_r diminishes, *KDL* increases logarithmically towards full dissociation.

Two important dimensionless quantities are $\Lambda_N \equiv k_{gr}/N_0$ and $\Lambda \equiv k_{gr}/n_0$, where, for the usual uni-univalent situation considered here, $n_0 = p_0 = c_0$, the common concentration of dissociated charges of mobilities μ_n and μ_p. Further, define the mobility ratio as $\Pi_m \equiv \mu_n/\mu_p$, and for the explicit one-mobile case we set $\mu_p = 0$. It immediately follows from the results of [4] that the important dissociation ratio, $D_D \equiv n_0/N_0$, may be expressed as

$$n_0/N_0 = \Lambda_N/\Lambda = \Lambda/(1+\Lambda) = \Lambda_N/[(\Lambda_N/2) + \{(\Lambda_N/2)^2 + \Lambda_N\}^{1/2}]. \quad (1)$$

For Λ_N values of 0.001, 0.1, and 10, D_D values are about 0.0311, 0.270, and 0.916, respectively, covering the transition from small to nearly full dissociation and resulting in an appreciable increase in M over this range. If we set $N_0 = 10^{16}$ cm^{-3} and $k_g = 1$, as in [10], then the above Λ_N values correspond to k_{gr} ones of 10^{13}, 10^{15}, and 10^{17} cm^{-3}, respectively, and thus to *KDL* values of 13, 15, and 17.

In the original main version of the LEVM general [4] computer program for impedance, its fitting parameters did not explicitly include all three k_g, k_r, and N_0 parameters, and mobilities appeared for one choice only through their presence in Π_m and in R_∞, the inverse of the high-frequency limiting quantity G_∞, here given by $G_\infty = (A/L)(e\mu_n n_0)(1 + \Pi_m^{-1})$, where e is the proton charge. Therefore, the program has been modified to involve such quantities explicitly for easy comparison with the results of [10]. One version of the present Circuit-H PNP model available in LEVM includes the following parameters: N_0, M, Π_Z, Π_m, k_{gr}, ξ, C_∞, μ_n, L, A, and ε_∞. Here A is the electrode area, and C_∞, the high-frequency limiting capacitance, often designated the geometrical, primarily dipolar, capacitance, C_g, is defined as $(A/L)\varepsilon_V\varepsilon_\infty$, where ε_V is the permittivity of vacuum. The parameter ξ is the ratio of the recombination relaxation time, τ_{GR}, to the Debye one, here denoted as $\tau_P \equiv R_\infty C_\infty$.

When $\Pi_m = 1$, the generation and recombination parameters play no role, but Λ_N and ξ are important quantities under other conditions. Because of their inter-relations, not all of the parameters listed above can be simultaneously set free during CNLS fitting. An example of an inter-relation following from the present definitions is $\xi/k_{gr} = (e\mu_n/\varepsilon_V\varepsilon_\infty)$ for the one-mobile situation, a result that leads to the equality $\Lambda = \tau_{GR}$. Although there are too many parameters to show all responses here, a few complete-blocking responses are included below. It is important to mention that because the complete GR equations are instantiated in the freely available LEVM Circuit-H model, it is trivially easy to use it to generate accurate GR transient response and frequency response and plots at any of the four immittance levels. Even more important, this model is currently unique in allowing the full GR model to be fitted by CNLS to experimental data to estimate model parameter values.

An apparent difference between the approaches of [7, 10, 26] and those in [4, 25] is that the results in the earlier work were first expressed in terms of the physically significant diffusional/interface dispersed part of the response and then combined with the high-frequency limiting resistance and capacitance quantities to form the final impedance expression, while no such separation was made in the later works cited above. Their impedance equation for the special two-mobile case with $\Pi_m = 1$ agrees with that of earlier more general work [2], and their one-mobile case is well approximated by a choice of $\Pi_m \geqslant 10^{40}$. Although GR effects are significant in the two-mobile situation except when $\Pi_m = 1$, Derfel *et al* [10] and Barbero and Lelidis [26] only presented graphical results for the one-mobile case with variable GR effects and did not present general two-mobile response results.

To investigate one-mobile responses and compare with the results of [10], LEVM was first used to generate synthetic results for the same input parameters as those employed in [10]. These values were $L = 2.5 \times 10^{-3}$ cm, electrode area, A, of 2 cm^2, diffusion coefficient $D = 8.2 \times 10^{-7}$ $cm^2\ s^{-1}$, $N_0 = 10^{16}$ cm^{-3}, $T = 290.11$ K, and $\varepsilon_\infty = 6.7$. From the Einstein relation, their corresponding μ_n value is 3.28×10^{-5} $cm^2\ V^{-1}\ s^{-1}$. For the present parameter values $\xi/k_{gr} = 8.8585 \times 10^{-12}$.

Figure 4(a) shows some wide-range frequency response results for six one-mobile choices and three two-mobile ones in order to compare with the results of [10] and to show some PNPA and GR effects not considered therein. The one-mobile PNP curves with *KDL* values of 13, 15, and 29 shown here correspond to comparable ones in [10]. Note that for *KDL* = 13, however, PNPA results are included for $\psi = 0.99$ and 0.90. The low-frequency window is here extended to frequency values less than generally experimentally available in order to demonstrate that while two plateaus are possible for one-mobile situations [10, 25, 26], three may appear for two-mobile ones [4, 25]. The present wide range, and possibly even lower frequencies, may also be of interest because GR response with $\Pi_m \gg 1$ might sometimes be a factor in observed impedance-spectroscopy long-time temporal hysteresis.

The highest-frequency $R'(\nu)$ plateau height here is just that of R_∞, and the one-mobile R_0/R_∞ curve of figure 4(b) shows that the low-frequency R_0 plateau may exceed R_∞ by a factor greater than 13, and that their ratio approaches unity in the limit of both zero and full dissociation. Particularly interesting is the non-monotonic behavior of R_0 versus *KDL* in the region from 14.5 to 15.5, not evident in the numerical results presented in [10]. But the valuable later work of [26], including an explicit expression for R_0, has fully verified the R_0/R_∞ response curve of figure 4(b), and appreciable further one-mobile GR results are included in [26] that both confirm and expand some of the present results. The recombination quantity k used in [26] corresponds to $-(KDL + 6)$ in the present work.

Barbero, one of the authors of [10], who has been very helpful with the present comparisons, kindly sent me several one-mobile $Z(\nu)$ full synthetic one-mobile data sets calculated

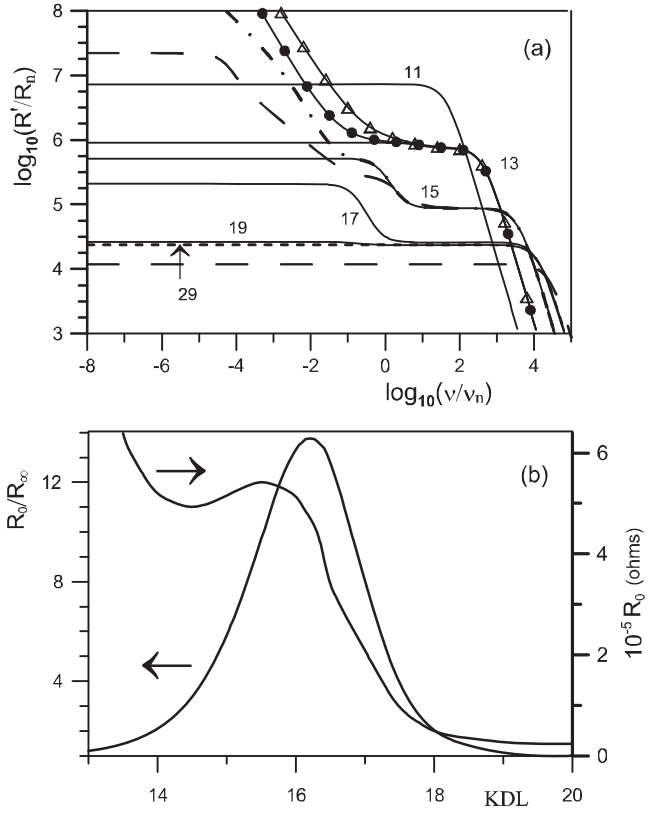

Figure 4. (a) Log–log plots of wide-range exact PNP and PNPA responses of $R'(\nu)$ for various parameter choices demonstrating generation–recombination and mobility-ratio effects. Here the normalization quantity R_n is 1 Ω. The LEVM Circuit-H fitting program was used to generate data with parameter values equal to those employed in [10] and discussed in section 2.2. All solid lines without symbols are one-mobile responses with their generation–recombination situations identified by a *KDL* value (see section 2.2) and all with $k_g = 1\ s^{-1}$. The $KDL = 13$ line with solid dot symbols and that with open triangles involve PNPA ψ values of 0.99 and 0.9, respectively. For all other responses, $\psi = 1$. The long-dash and dash-dot lines for the $KDL = 15$ situation are two-mobile-type responses for Π_m values of 10^3 and 10^5, respectively. The $KDL = 29$ short-dash curve shows fully dissociated one-mobile response. The bottom long-dash line is that for the two-mobile $\Pi_m = 1$ situation. (b) R_0/R_∞ and R_0 dependences on *KDL*, where R_0 is the low-frequency-limiting value of the $R'(\nu)$ plateau for one-mobile PNP responses and $R_\infty \equiv 1/G_\infty$ where G_∞ is the high-frequency limiting value of $G'(\nu)$.

with equation (68) of [10] and involving the one-mobile Debye length, L_{D1}, defined in appendix A.3. Note that $L_{D1} = \sqrt{2}L_{D2}$, so $M_2 = \sqrt{2}M_1$. These data sets were first fitted using LEVM with the two-mobile [4] model of equation (32) using a value of $\Pi_m = 10^{40}$ or greater, and then with the strict one-mobile model of equation (8) of [25], the same as that of equations (24) and (40) of [4]. All such fits for each value of *KDL* were identical and led to exceptionally small values of the relative standard deviations of the fit residuals, S_F, of the order of 10^{-6} and also to the expected input parameter estimates with relative standard deviations of the same order, full verification of agreement of the [10] results with the earlier response equations.

Although the epsilon-level response shows much less effect of GR than does the impedance-level one, there are a few interesting details. First, its complex-plane response is that of a Debye half-circle for *KDL* values of 11 or less and for ones of 19 or more. In the region from 14 to 18, the original semicircle begins to undergo behavior like mitosis: its shape distorts until a smaller semicircle begins to appear at frequencies lower than those of the original one. This smaller semicircle is of maximum size for *KDL* near 15 and then decreases as *KDL* increases. Behavior of this sort is shown in figure 5(a) of [6]. As shown in equation (9) of [25], it results in a low-frequency increase in ε_0 over its higher-frequency plateau value by a factor that reaches $\sqrt{2}$ in the limit of zero dissociation. No such increase occurs for the two-mobile situation with equal mobilities.

The one-mobile behavior is quantified by the following result for $\varepsilon_{0N} \equiv \varepsilon_0/\varepsilon_\infty$ [4, 25]. First define $G_L \equiv [(2 + \Lambda)/(1 + \Lambda)]^{1/2}$ and $r_0 \equiv M_1 G_L \mathrm{ctnh}(M_1 G_L)$. Then $\varepsilon_{0N} = r_0$. For full dissociation, Λ and *KDL* become infinite and $\varepsilon_{0N} = M_1 \mathrm{ctnh}(M_1)$. In the opposite limit of zero dissociation and full recombination, Λ goes to zero and *KDL* to $-\infty$, so $\varepsilon_{0N} = M_2 \mathrm{ctnh}(M_2)$. For $M > 3$, the ctnh term may be set to unity. These results show that, for full dissociation in the one-mobile situation, charge of only one sign is mobile, but as the dissociation ratio becomes small, generation–recombination eventually leads to full effective mobilization of the fixed charges, two-mobile behavior. Although this physical interpretation is discussed in [4, 25], it is not mentioned in [10] although its equation (77) is equivalent to the above general expression for ε_{0N} when $M_1 > 3$. In summary, the work of [10, 26] have been shown to be consistent with earlier more general GR analyses, ones incorporated as fitting models in LEVM.

Finally, it is worth again mentioning that at least in some situations, PNP model double layers may explain the appearance of colossal low-frequency dielectric constants. A substance showing such effects that has been appreciably studied is $CaCu_3Ti_4O_{12}$ [29–31]. Lunkenheimer has kindly sent me frequency response data for this material in single-crystal form with sputtered gold electrodes [32]. A good fit of the 140 K data with a composite model including the PNPA was found and led to $\psi \cong 0.9$ and to $M \cong 754$. The ε_∞ estimate was about 85 and good agreement was found between the large PNP ε_0 value and $M\varepsilon_\infty$. A small rise in $\varepsilon'(\nu)$ at the low-frequency part of the response, identified in [29] as a second relaxation, was very well fitted with the above anomalous diffusion value of ψ and possibly arises from electrode roughness, a more likely possibility than that it is associated with GR effects.

3. Fit results for a hydrogel

Alexe-Ionescu kindly provided room-temperature response data for a gel of composition 1% ethylene glycol, 1% hydroxyethylcellulose, and 98% depurated water [27]. This data set exhibits some mobile-ion conduction, possibly arising from impurities in the hydroxyethylcellulose component of the material. Table 1 summarizes fitting results of this data set for various composite models involving DebD, Deb, PNP, or PNPA functions. See the appendices A.2 and A.3, for

Table 1. LEVM CNLS proportional-weighting fits with various composite models at the epsilon immittance level for specific frequency response data for a gel of composition 1% ethylene glycol, 1% hydroxyethylcellulose, and 98% depurated water (in weight), measured with silver-plated electrodes. Its cell constant, CC, was 9.479 cm and the electrode separation L was 0.53 mm. The original data contained obvious systematic errors which were removed. Models are written using impedance-parameter names but all fits are of data in specific form. The GPNP · Deb designation indicates a conductance G (specific name $\sigma' \equiv \sigma_P$) in parallel with a bulk microscopic PNP model, and the combination in series with a resistivity-level Debye model (Deb). A Debye response model defined at the dielectric level is designated DebD here. The letter F indicates a fixed parameter value and C a calculated value using, for example, $\varepsilon_0 = M\text{ctnh}(M)\varepsilon_\infty$ for the PNP but not the PNPA model, and $\rho_\infty = \tau_D/(\varepsilon_V \Delta\varepsilon_D)$ for the DebD model.

#, Model	S_F and PDRMS	$10^{-3}\rho_\infty$ (Ω cm)	$10^8\tau_P$ or $(10^3\tau_D)$ (s)	$10^{-4}M$	ψ	$10^5\sigma_P$ (S cm^{-1})	$10^{-3}\rho_D$ and $10^{+3}\tau_D$	ε_∞; and $10^{-6}\varepsilon_0$ for PNP only
1 PNP	0.171	8.21	8.05	4.07	1F	—	—	110.7
	0.036						—	4.50C
2 CDebD	0.171	8.21C	(3.27)	—	—	—	—	110.7
	0.036						—	4.50
3 GPNP	0.095	9.89	9.65	2.57	1F	2.39	—	110.2
	0.037						—	2.84C
4 PNPA	0.091	8.28	7.78	1.09	0.858	—	—	106.1
	0.039						—	—
5 PNP · Deb	0.063	8.29	8.03	8.41	1F	—	7.58	109.3
	0.046						3.86	9.93C
6 GPNPA	0.055	9.37	8.91	1.27	0.907	1.68	—	107.4
	0.036						—	—
7 PNPA · Deb	0.052	8.22	7.85	8.41	0.892	—	7.58	109.3
	0.074						3.86	—
8 GPNPA · Deb	0.037	9.57	9.21	3.82	0.995	1.87	1.62	108.7
	0.087						1.14	—
9 GPNP · Deb	0.037	9.59	9.23	4.02	1F	1.90	1.66	108.7
	0.052						1.14	4.37C
10 GCDebD · Deb	0.037	9.59C	(3.72)	—	—	1.90	1.66	108.7
	0.052						1.14	4.37

information on these models and their fitting parameters, and note that the fully dissociated PNP model used here involves only three free fitting parameters, so either, but not both, of ε_∞ and τ_P are taken free at the same time. Fit results with several other models were much poorer than those shown in the table.

In the table S_F is a measure of the relative standard deviation of the fit residuals and PDRMS is the RMS value of the estimated relative standard deviations of the free fit parameters. For a good fit, one would expect both quantities to be of the order of 2% or less. Although the results in table 1 do not well meet this criterion, figure 5, which shows results for the row-9 fit in the table, demonstrates rather good agreement between the data and the GPNP · Deb model, as well as consistency with the synthetic data plots of figures 2 and 3. Inclusion of the significant G part of the model, represented by the free parameter σ_P, indicates the presence of partial rather than complete blocking. It might be associated with the same ions that lead to $\rho_\infty \equiv 1/\sigma_\infty$ and, if so, the thermal activation energies of these quantities would be equal.

Although the goodness-of-fit measures for the present data are of the order of four per cent or larger, possibly because of some remaining systematic errors in the data, on what basis should we pick an appropriate fitting model? Clearly, if the goodness-of-fit values for one model were significantly better than those of any others investigated, it should be considered first, particularly if it involves fewer free parameters, all of which were of physical significance.

It is well known, however, that discrimination by external measurements between conduction and displacement currents is impossible [16, 33]. The problem is well illustrated by the results discussed below of rows 1 and 2 and by 9 and 10 in the table, where the fits are equally good but those of lines 1 and 9 involve bulk resistive relaxation/dispersion and those of 2 and 10 involve bulk dielectric relaxation. We nevertheless pick the row-9 ionic conduction results for further consideration here since the present work deals primarily with PNP and PNPA relaxation and dispersion. Further, as discussed above, if the two resistive parameters of the GPNP model were found to have essentially equal activation energies, it would be reasonable to identify the bulk relaxation response of the system as involving resistive rather than dielectric behavior. Data for the present hydrogel material over a range of temperatures could answer this question.

Note that the PNP model τ_P estimates of table 1 are much smaller than the τ_D ones of the series Deb one, indicating that the Deb model makes its fit contribution primarily in the lower-frequency range. In fact, its effect is a relatively minor one, and plots of either the GPNP part of the GPNP · Deb fit or of a GPNP fit alone both show only small deviations between the full fit and the data shown in figure 5. Thus, the GPNP model alone can reasonably well fit experimental $\varepsilon(\nu)$ data that leads to exceptionally high $\varepsilon_0 \equiv \varepsilon'(0)$ values, here associated with double-layer formation, such as the experimental results discussed in section 2.1. Curves such as that in figure 5 for σ'' are often observed with the left peak associated with electrode polarization effects since such a peak disappears when only a bulk conductive-system model such as the CK1 is considered [21, 34].

Figure 6 shows complex-plane plots of the data, fits, and separate fit parts for both the ρ and the σ levels. Such plots,

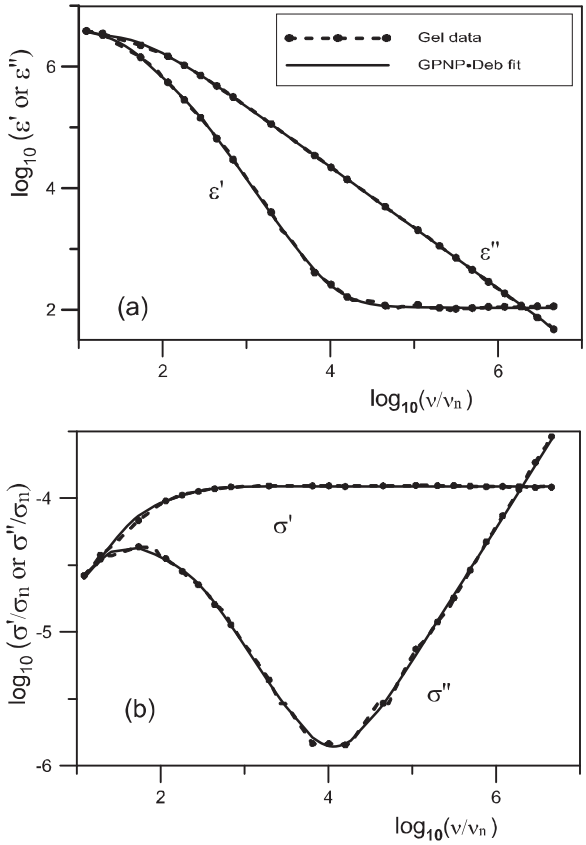

Figure 5. Log–log plots of GPNP · Deb fits for the gel data of table 1, row-9. (a) $\varepsilon'(\nu)$ and $\varepsilon''(\nu)$; (b) $\sigma'(\nu)$ and $\sigma''(\nu)$.

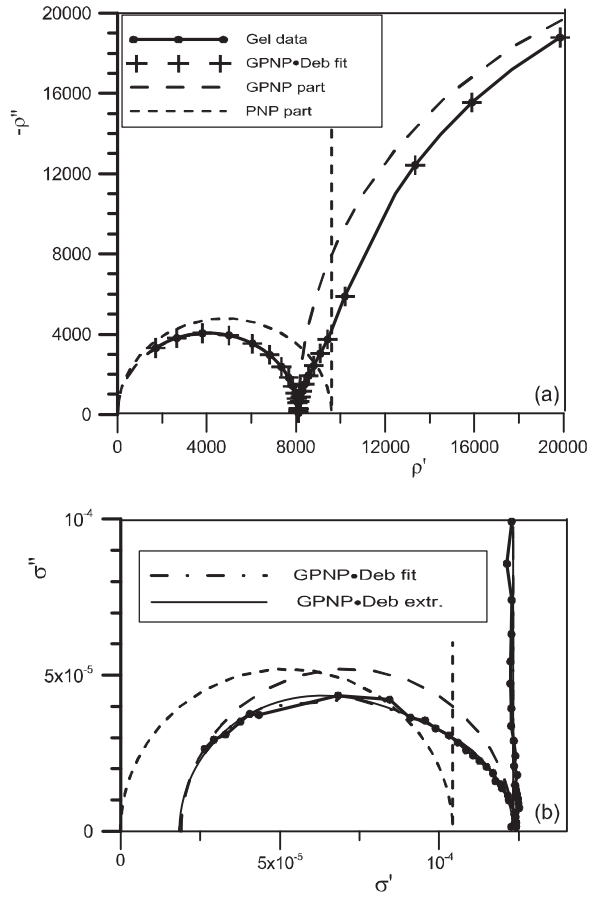

Figure 6. Complex-plane plots for the gel data fits of table 1, row-9, showing (a) ρ and (b) σ data and fits and the responses of the individual parts of the composite fit model.

being of linear–linear form, show differences between data and fit results better than do log–log ones, such as those of figure 5. Here low-frequency results are at the right side of figure 6(a) and show full blocking for the PNP part of the fit but not for the full data or for the GPNP part. In contrast, for figure 6(b) high-frequency results are at the right and the vertical lines show the regions where $\sigma'(\nu) = \sigma_\infty$. Clearly, the results of figure 6(b) show more differences between fit results and data than do those of figure 6(a).

The poor-fit results shown in the table for rows 1 and 2 are identical and show that for large M values, as here, a conducting-system PNP data set is undistinguishable from a dielectric-system CDebD one [16, 33, appendix 3], but we assume that we are dealing with a relaxing/dispersive material involving diffusing ions, so only the former is then appropriate. The fit results for the first 4 rows of the table are all somewhat unsatisfactory, but we see that including a G conductivity element in parallel with the main bulk response, and/or including a series Debye element, all appreciably improve the fits.

It is interesting to note that the row-3 and row-6 results for normal and anomalous diffusion lead to M values that differ by very close to a factor of two. On comparing the results for the row-6 and row-8 fits, one sees that the latter leads to a PNPA ψ value very close to unity, and therefore that the row-9 results are clearly more appropriate. Finally, comparison of the row-9 and row-10 results again shows that no discrimination on the basis of fitting results alone is possible here between the conducting-system fit of row-9 and the dielectric-system one of row-10. It also demonstrates that data which might be expected to be of pure dielectric-system character can be well fitted by an appropriate conductive-system model [16, 33].

Note that the ε_∞ estimates in the table are all of the order of 109, rather than an expected value for this material of slightly less than that of pure water. It seems likely that this discrepancy arises from the effective area of the electrodes being larger than their measured values, a common occurrence (e.g., [35]). If we reduce the cell constant used in transforming to specific data form by a factor of 1.394 at the dielectric level, the new row-9 results then involve an ε_∞ estimate of 78, and τ_P, M, and the $\rho_\infty\sigma_P$ product all remain the same, as expected.

Equations (A.8) and (A.9) yield estimates of the diffusion coefficient, D, and the Debye length, L_D, independent of the cell constant when $\Pi_m = 1$ and when estimates of L, M, and τ_P are available, not true for the calculation of L_D from its usual definition because ε_∞ and temperature are then directly involved. For the large-M row-9 results, we obtain the plausible estimates $D \simeq 4.7 \times 10^{-6}$ cm^2 s^{-1} and $L_D \simeq 6.6 \times 10^{-7}$ cm. But more analysis and understanding of the present data can be obtained by using the general PNP/PNPA fitting program described in section 2.2.

We begin by using the PNP parameter values in row-9 of table 1 to generate exact complex response data. Its fitting

for full dissociation with equal mobilities and then also with one of them very close to zero, the one-mobile case, led to the M value shown in row-9 (M_2) and to $\sqrt{2}$ times that value (M_1), respectively, as expected [25]. Using a fitting choice that allows N_0, n_0, μ_n, L, and ε_∞ parameters to be estimated and setting $T = 300$ K, one obtains for the two-mobile situation the following estimates: 1.79×10^{18}, 1.79×10^{18}, 1.82×10^{-4}, 0.053, and 108.7, respectively, with the usual units. Here, since we are dealing with full dissociation, the first two values are identical. For the present temperature choice, the μ_n estimate leads to a D value of about 4.3×10^{-6} cm^2 s^{-1}, perhaps suggesting that the actual temperature of the measurements was lower than 300 K, but we will use this value nevertheless. Fitting the same data with the one-mobile choice led to larger estimates of all parameters except ε_∞. Since the resulting L estimate was about 0.075 cm, a factor of $\sqrt{2}$ larger than the proper value, it is clear that the two-mobile choice is the proper one here since it yields a close approximation of the known input value of L.

Next we carry out a two-mobile fitting of the above type using the actual experimental hydrogel data. A parallel resistivity, $\rho_p \equiv 1/\sigma_p$, needs to be included to represent the GPNP model used in row-3 of table 1. The fit results were 1.82×10^{18}, 1.82×10^{18}, 1.74×10^{-4}, and 110.2, with L fixed at 0.053 cm and a ρ_p estimate of 4.18×10^4 Ω cm.

The fit results for the GPNP · Deb situation like that of row-9 of table 1, were the same as those found there and as those for the exact PNP data listed above, with L again fixed at 0.053 cm and a ρ_p estimate of 5.27×10^4 Ω cm. For this somewhat noisy data it was not found possible to obtain fit estimates of N_0, μ_n, and L values with all three simultaneously free to vary, but with any one of them fixed the others could be well estimated. Similarly when the mobility ratio was taken to be an additional free parameter its estimate was 1.000 ± 0.014.

The N_0 estimate of 1.79×10^{18} cm^{-3} is not unreasonable for a ρ_∞ value of about 10^4 Ω cm, but it cannot be independently estimated because the type of mobile ions present in the gel was not identified. The relatively small value of the low-frequency resistivity suggests that full dissociation of impurities might be the ion source. Finally, it seems likely that for good fits, the use of the present fitting model to estimate the mobile-ion density, n_0, from σ_∞ or L_D values might often be more appropriate than estimating it from the Nernst–Einstein equation using an uncertain value of the hopping rate [36].

4. PNP analyses of synthetic data sets

Some recent results of Serghei *et al* analyzing liquid-electrolyte data [28] led to the interesting and potentially useful equation

$$\sigma_0 = 2\pi\varepsilon_V\varepsilon_\infty(\nu_0^2/\nu_m), \tag{2}$$

where ν_m is the frequency at the left peak of a σ'' curve such as that in figure 5 and ν_0 is the frequency of the minimum at the right that follows this peak. Further, σ_0 is defined in [28] as the dc conductivity at the interface and thus corresponds not to any non-zero dc $\sigma_{dc} \equiv \sigma'(0)$ conductivity but to the plateau value defined here as σ_∞. Although not mentioned in [28], it is possible to simplify equation (2) by using equation (A.4), yielding the more transparent result

$$\tau_D\langle\tau/\tau_D\rangle = (\omega_m/\omega_0^2), \tag{3}$$

where the normalized mean relaxation time of the model, $\langle\tau/\tau_D\rangle$, is just γ_{DC} for the Davidson–Cole response model [18, 37].

The PNP model intrinsically includes interface effects, as discussed in sections 2 and 3 and in appendix A.3, and thus it does not require an additional capacitance in series to ensure complete blocking at the electrodes. In contrast, the work of [28] employed a composite model made up of a conductive-system bulk one (not the PNP) and a series electrode-polarization model of identical form. For such a partial-blocking approach, equation (2) only applies when both parts are present, since for the bulk one alone the σ'' response shows no minimum and peak [34]. In [28] the relationship

$$\tau\,(\text{interface})/\tau\,(\text{bulk}) \cong \sigma_0(\text{bulk})/\sigma_0(\text{interface}) \gg 1, \tag{4}$$

was used with an actual value of this ratio of 1.3×10^8, and this relation was stated to have a solid physical justification. It is, in fact, inapplicable for complete-blocking situations; neither the $\cong$ sign nor this particular value are general; and all four parameters are best determined for an experimental partly blocking data set by CNLS fitting with an appropriate composite model.

To further explore this matter, first let us use a GPNP · Deb model to generate synthetic data like that of row-9 of table 1, with $\sigma_\infty = 10^{-4}$ S cm^{-1}; $\varepsilon_\infty = 100$; $\tau_P = 8.854\,19 \times 10^{-8}$ s; $\sigma_P = 1.898\,73 \times 10^{-5}$ S cm^{-1}, the G parameter; $M = 4.0 \times 10^4$; and the Deb values listed in row-9. Accurate estimates of ν_m and ν_0 are ensured by the use of numerous closely spaced data points. We find that the actual plateau value, σ_{0P}, is about 1.19×10^{-4} S cm^{-1}, not equal to σ_∞, and equation (2) yields $\sigma_0 = 1.76 \times 10^{-4}$ S cm^{-1}, nearly 50% larger even than σ_{0P}. When just the GPNP model is employed, however, the actual plateau value is the same as σ_{0P} and equation (2) yields just 10^{-4}, the correct σ_∞ value of the PNP model but not the actual plateau value of the GPNP one. Finally, for just the PNP model, the absence of the G parameter, which only affects σ'-level but not σ''-level data, leads to both the original plateau value equal to the model σ_∞ and to its proper estimate using equation (2). Since the gel modeled by PNP is 98% water, we expect that it is sufficiently liquid-like that equation (2) might well apply, as it does. In fact, although only data for ionic liquids are analyzed in [28], it does not explicitly restrict equation (2) to liquids, and I have found that equations (2) and (3) apply for all materials investigated so far whose data extend to low enough frequencies to include the characteristic ν_m peak and ν_0 minimum.

In order to test equations (2) and (3) using CNLS fitting for a representative ionic-liquid data set with other models, such as the PNP, I requested that the authors of [28] send me one of the data sets employed in that work. When no response was received, I constructed an exact synthetic data set somewhat similar to both the present gel data and to one of those in [28]. Its parameter values are listed in the caption of table 2 and in its

Table 2. LEVM CNLS proportional-weighting fits of exact specific data generated from a Deb · DC0 model at the epsilon immittance level. The interface Deb parameters are shown in row-1 of the table and the bulk DC0 parameter values were $\rho_{DC} = 10^5\ \Omega$ cm, $\tau_{DC} = 10^{-6}$ s, and $\gamma_{DC} = 0.7$. In the row-2 through row-7 fits shown here when the DC0 parameters were taken free to vary, their relative standard deviations, and those of $\sigma_P \equiv \sigma_{DD}$, here 10^{-10} S cm^{-1}, were always of the order of 10^{-9} or smaller, so they were fixed and are not listed below. Number of data points: 111 for rows 1–8, 80 for 9 and 10, and 71 for row 11 (maximum frequencies 10^8, 8×10^4, and 10^4 Hz, respectively). *C* designates a value calculated from DC0 parameters, and C_p from PNP ones.

#, Model	S_F and PDRMS	(ρ_{DC}) or ρ_∞ (Ω cm)	(τ_{DC}), $\{\tau_{DD}\}$, or τ_P (s)	M Mctnh(M)	ε_∞ and ε_0
1 Deb · DC0	Exact	(10^{10})	(10^3)	—	79.059*C*
	—			—	$1.1294 \times 10^6 C$
2 CDebD · DC0 A	1.1×10^{-12}	—	$\{7.86 \times 10^{-15}\}F$	—	98.22
	7.0×10^{-6}		or $\{0\}F$	—	1.1293×10^6
3 GPNP · DC0 B1	5.7×10^{-10}	3.23×10^{-6}	7.86×10^{-15}	41.11	—
	1.9×10^{-3}			41.11	—
4 GPNP · DC0 B2	5.7×10^{-10}	3.24×10^{-6}	—	41.16	—
	1.1×10^{-3}			41.16	2.744×10^4
5 GPNP · DC0 C1	3.7×10^{-10}	7.90	7.90×10^{-7}	0.038 60	$1.1283 \times 10^6 C_p$
	5.4×10^{-4}			1.000 50	$1.1289 \times 10^6 C_p$
6 GPNP · DC0 C2	2.7×10^{-10}	7.69	$7.69 \times 10^{-7} C_p$	0.035 84	$1.1278 \times 10^6 C_p$
	2.9×10^{-4}			1.000 43	1.1289×10^6
7 GPNP · DC0 D1	1.7×10^{-8}	1.77×10^3	1.76×10^{-4}	0.133 63	$1.1160 \times 10^6 C_p$
	4.9×10^{-3}			1.005 98	$1.1227 \times 10^6 C_p$
8 GPNP · DC0 D2	1.3×10^{-2}	7.89×10^4	$8.48 \times 10^{-7} C_p$	9.305×10^3	121.4
	1.8×10^{-2}			9.305×10^3	1.1292×10^6
9 GPNP E1	2.8×10^{-3}	9.992×10^4	6.97×10^{-7}	1.434×10^4	$78.81 C_p$
	6.7×10^{-4}			1.434×10^4	$1.1298 \times 10^6 C_p$
10 GPNP E2	2.8×10^{-3}	9.992×10^4	$6.97 \times 10^{-7} C_p$	1.434×10^4	78.81
	6.4×10^{-4}			1.434×10^4	$1.1298 \times 10^6 C_p$
11 GPNP E3	4.7×10^{-5}	1.0001×10^5	$7.00 \times 10^{-6} C_P$	1.429×10^4	79.046
	1.6×10^{-5}			1.429×10^4	$1.1294 \times 10^6 C_p$

row-1, and its frequency responses for three immittance levels are presented in figure 7 in order to allow direct comparisons of the results at these levels. The composite model $\text{Deb}_i \cdot \text{DC0}_b$ was used in place of a $\text{Deb}_i \cdot \text{Deb}_b$ one in order to include the high-frequency rise in $\sigma'(\nu)$ shown in figure 7(a) and apparent in the figure 3(c) plot of [28], but not discussed there. Here the i and b subscripts indicate interface and bulk quantities. Note that the fit results of row-9 of table 1 and those of rows 1 or 8 of table 2 fail to satisfy the $\cong$ requirement of equation (4).

The exact $\text{Deb}_i \cdot \text{DC0}_b$ parameters were used to generate closely spaced $\sigma''(\nu)$ data points to allow accurate estimates of ν_m and ν_0: 15.916 and 1901.9 Hz, respectively. The ν_m value is also equal to that of the peak value of the $\varepsilon''(\nu)$ curve of figure 7(b), ε_{pk}, and the ν_0 one is the same as that of the minimum of the $\rho''(\nu)$ curve of figure 7(c). For the $\text{Deb}_i \cdot \text{DC0}_b$ exact model data of row-1 of table 2, equation (2) leads to $\sigma_{DC} = 0.9996 \times 10^{-5}$ S cm^{-1}, and equation (3) to $\tau_{DC} = 1.0004 \times 10^{-6}$ s, very good approximations to the corresponding input values and an indication that equation (2), and (3) apply exactly to appropriate data.

The row-2 results of table 2 show that although a CDebD composite model, in place of the original Deb part of the total fitting model, led to nearly a perfect fit, it nevertheless did not yield either a close estimate of ε_∞ or a meaningful estimate of its τ_{DD} parameter. Rows 3–6 further demonstrate that with a GPNP interface model in series with a DC0, one can also obtain excellent fits but essentially meaningless parameter estimates except that for ε_∞.

Results are a little better but still unsatisfactory for row-7, where the DC0 parameters are fixed at their input values. When they were free to vary, however, as in row-8, there are seven free parameters; the overall fit is much worse but still acceptable; and the parameter estimates are closer to proper values. The estimate of σ_p was exact and those of ρ_{DC}, τ_{DC}, and γ_{DC} were $2.12 \times 10^4\ \Omega$ cm, 2.03×10^{-7} s, and 0.633, respectively. When the frequency window was reduced to an upper limit of about 8×10^4 Hz, the results shown in rows 9 and 10, where no DC0 needed to be included in the fit model, led to an appreciably improved fit and to parameter estimates very close to expected values. Finally, when the maximum frequency was limited to 10^4 Hz, row 11 shows an even far better fit and very close parameter estimates.

The authors of [28] show in their figure 2(f) some dependence of their σ'' peak response on the composition of the metal of the electrodes. Because they found that their data sets for different metals were consistent with the present equations (2) they concluded that 'the current theoretical approach renders the correct explanation for the dependence on the material of the electrodes'. This sweeping statement, along with their claim that their approach provides a microscopic understanding of the phenomenon, seems inappropriate because it does not consider the details of physical processes and conditions involved at the surface of the metals, such as atomic-scale inhomogeneities, oxide layers, etc (e.g., [29, 30, 35, 38, 39]).

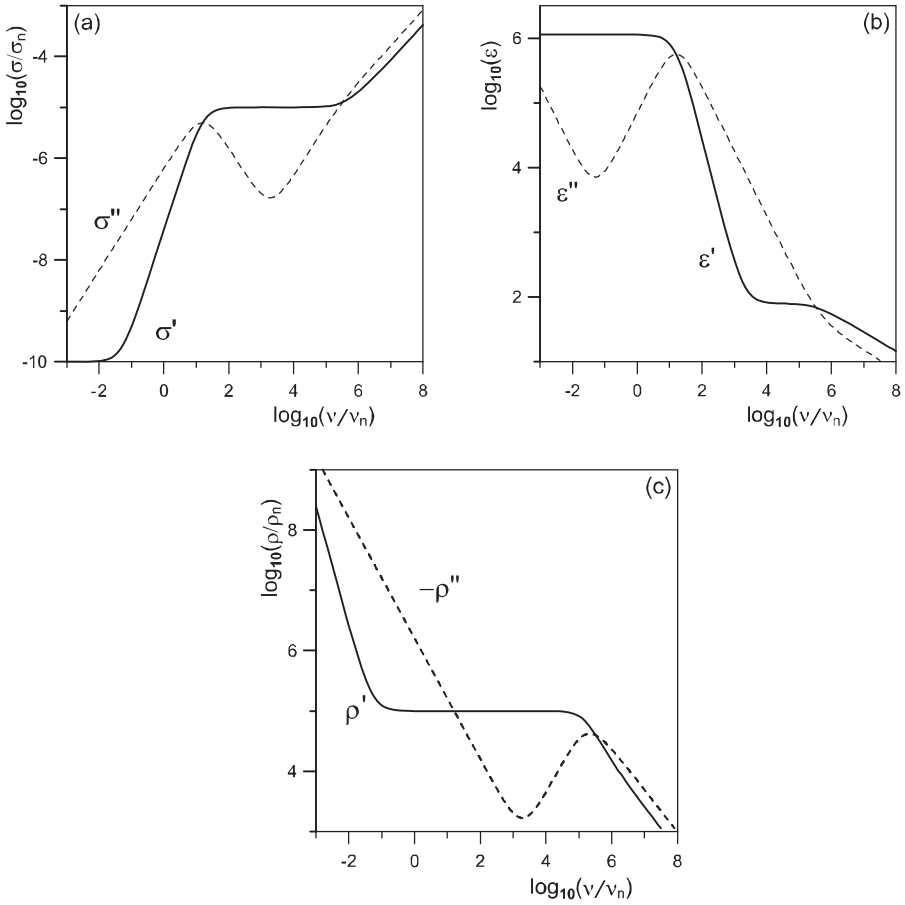

Figure 7. Log–log plots of the exact Deb · DC0 data of Row-1, table 2 showing (a) $\sigma(\nu)$, (b) $\varepsilon'(\nu)$, and (c) $\rho(\nu)$ real and imaginary parts. All fits in the table are indistinguishable from the data. Here $\rho_n = 1\ \Omega$ cm.

5. Some possible limitations of PNP/PNPA models

When $0 < \psi < 1$, the PNPA model involves anomalous diffusion and at constant temperature the capacitance increases continuously as the frequency decreases in the low-frequency region until it eventually becomes limited by the largest effective τ present in the relevant distribution of relaxation times or by steric effects. Although even the PNP model, involving point charges, seems able to well fit colossal dielectric constant data, as discussed in section 2.1, there are certainly steric limitations to the maximum dielectric constant associated with realistic diffuse double layers involving finite-size ions. The present continuum model does not include a finite-ion-size compact Stern inner layer at each electrode, most appropriate for liquids but still possible for solids.

The steric effects of finite-size ions have been widely discussed in various ways for many years. Some of the early work is cited and discussed in [11, 40] but that in [41–47], carried out in the period 1962–1992, is also relevant. Further, in [48] the authors cite several studies dealing with modifications of the Poisson–Boltzmann equation and propose a simple change in the basic PNP microscopic equations for ionic transport that at least qualitatively accounts for steric effects. In important recent work that also discusses further modified-Poisson–Boltzmann equations [49], simulations of probing the electric double layer at a metallic electrode/electrolyte interface are reported that seem able to provide some direct evidence of spatial charge distribution in the diffuse layer.

The results of recent molecular dynamics and PNP/Stern simulations [50] suggest that a compact layer might lead to a series capacitance per square centimeter of electrode area of the order of 1 μF, but because the effective area for supercapacitors is much larger than their geometric area, the limiting value for such situations could be far larger. So far, no need has been found, in fitting experimental data using the present PNP or PNPA models, for the addition of a series inner-layer capacitance in the fitting model, probably because such capacitance is much greater than the estimated diffuse double-layer capacitance following from such models.

In the final section of [25] it is concluded that GR theoretical predictions have a wide range of applicability for some physical situations, particularly those involving electronic conduction. But it is further suggested that significant GR effects may be small for most ionic materials. If we consider the $KDL = 16$ value of $R_0/R_\infty \simeq 13.3$ near the peak of the present figure 4 (b) curve of this quantity, we see that at least for the theoretical situation considered there, GR effects may indeed be significant, and the estimate of the value of this ratio using its equation (11) approximation of [25] is

close to the accurate numerical value following from both the present analysis and that of [26].

Clearly, one needs to find experimental situations where a significant low-frequency ionic plateau may be identified as arising from GR effects and quantified by fitting with a PNP or PNPA model. Good theory should be predictive but experimental verification is needed for its justification. As the distinguished physicist Richard Feynman said, 'Experiment is the sole judge of scientific truth'. But absence of evidence is not evidence of absence, and so much remains to be done.

Acknowledgments

I thank Professor Giovanni Barbero and his associates for many valuable comments and helpful suggestions, and I have also benefited from valuable inputs from Dr R F Hamou.

Appendix. Some data fitting models

A.1. Relevant relations and definitions

Since at least 1973, frequency response fitting models have been defined either at the dielectric constant (relative permittivity) level or at the impedance (resistivity) level, although the latter is still often termed dielectric response [14, 18, 21, 37]. As usual, we use Roman letters for the identification of quantities associated with both directly measured data and with the names of fitting models, and employ Greek letters for specific quantities. The word 'immittance', an intrinsically complex quantity, includes all four response levels: impedance Z, electric modulus M, admittance Y, and dielectric constant ε (or complex capacitance). For a measuring cell involving plane-parallel electrodes of area A and separation L, define $CC \equiv A/L$, and $C_G \equiv CC * \varepsilon_V$. Here CC is the cell constant; C_G is the geometric capacitance of the empty cell; and if the dimension of CC is cm, that of C_G will be Farads since the permittivity of vacuum. in Gaussian units is $\varepsilon_V \cong 8.85419 \times 10^{-14}$ F cm^{-1}.

Note that immittance quantities are related by $Y = 1/Z$ and $M = 1/\varepsilon$. Impedance data represented by Z is transformed to its specific corresponding complex resistivity quantity by $\rho(\omega) = CC * Z(\omega) = 1/\sigma(\omega)$. Therefore, a resistance R_∞ in ohms may be transformed to specific format by $\rho_\infty \equiv \rho'(\infty) = CC * R_\infty$. Further, $\sigma(\omega) = i\omega\varepsilon_V\varepsilon(\omega)$ and $M(\omega) = 1/\varepsilon(\omega) = i\omega C_g Z(\omega) = i\omega\varepsilon_V\rho(\omega)$. The high-frequency limiting capacitance of a filled measuring cell is $C_\infty \equiv CC * \varepsilon_V\varepsilon_\infty \equiv \varepsilon_\infty C_G$, involving the limiting, primarily dipolar, relative dielectric constant of the bulk material usually designated ε_∞ or $\varepsilon_{D\infty}$.

The four immittance levels for data in specific form are $\rho, M, \sigma, \varepsilon$. For dielectric data expressed at the ε level (dielectric response: $U = \varepsilon$, $k = D$) or conductive data at the ρ level (conductive response: $U = \rho$, $k = 0$ or 1), a general relation may be written as

$$I_k(\omega) = \frac{U_k(\omega) - U_k(\infty)}{U_k(0) - U_k(\infty)} = \int_0^\infty (-d\phi(t)/dt)\exp(-i\omega t)\,dt, \tag{A.1}$$

where $U_k(0) - U_k(\infty) \equiv \Delta U$; $I_k(\omega)$ is a normalized frequency response function; $I_k(0) = 1$ and $I_k(\infty) = 0$ for $k = D$ or 0 but not for $k = 1$; and $\phi(t)$ is correlation function [13, 14, 21, 23, 37]. The $I_k(\omega)$ function usually involves one or more shape parameters and a characteristic relaxation time, τ_0. For conductive-system response, $\rho(\infty)$ is usually found to be zero or negligible but for dielectric-system response ε_∞ is the non-zero high-frequency limiting bulk dielectric constant of the material, mostly dipolar in character and independent of mobile-ion concentration, at least at low concentrations.

Perhaps surprisingly, even a purely dielectric system leads to a non-zero low-frequency-limiting resistivity, one given by

$$\rho_{D0} = [(\Delta\varepsilon)_D/\{\varepsilon_V(\varepsilon_{D0})^2\}]\langle\tau\rangle_D, \tag{A.2}$$

but, of course, to a zero value of $\sigma_D(0)$ for completely blocking conditions [51][2]. Here, as usual, the D subscript indicates dielectric-system response, and $\langle\tau\rangle_D$ is the mean value of τ calculated using the dielectric distribution of relaxation times (DRT) for the fitting model. Similarly, for a conductive system the dual relation

$$\varepsilon_{C\infty} = [(\Delta\rho)_C/\{\varepsilon_V(\rho_{C0})^2\}]\langle\tau\rangle_C \tag{A.3}$$

applies, where $\varepsilon_{C\infty}$ is the high-frequency limiting dielectric constant of the material. In the usual case where $\rho(\infty)$ is negligible, it reduces to just

$$\varepsilon_{C\infty} = \langle\tau\rangle_C/[\varepsilon_V\rho_{C0}] = \sigma_{C\infty}\langle\tau\rangle_C/\varepsilon_V, \tag{A.4}$$

where we use $\sigma_{C\infty} = 1/\rho_{C0}$ since experimentally $\sigma'(0) = 0$ for completely blocking situations and for some models such as the PNP one.

A.2. Some empirical models

A widely used form of $I_k(\omega)$ is the Havriliak–Negami equation,

$$I_k(\omega) \equiv 1/[1 + (i\omega\tau_0)^\alpha]^\gamma, \tag{A.5}$$

where $k = D$ or 0 and α and γ are positive shape parameters that are usually 1 or less. When $\alpha = \gamma = 1$, this response function reduces to Debye relaxation, one involving a single relaxation time. Alternatively, when $\gamma = 1$ it represents Cole–Cole response, and when $\alpha = 1$, Davidson–Cole behavior, designated as DC0 or DCD [18, 37]. Note that for completely blocking situations only the DCD Davidson–Cole dielectric response model expressed at the σ level involves the physically correct limiting log–log power-law slope of two for $\sigma'(\omega)$ as $\omega \to 0$, as does its Debye limit, one where $\langle\tau\rangle_D$ reduces to $\tau_0 = \tau_P \equiv 1/\omega_P$, the peak of $\varepsilon''(\omega)$. Further, Cole–Cole response for conductive data, called the ZC model has been shown to be a poor fitting model and its frequently used real part is even less appropriate [52].

For the DC0 model with $\gamma = \gamma_{DC}$ and $\rho(\infty) = 0$, equation (A.4) reduces to

$$\varepsilon_V\varepsilon_\infty = \sigma_\infty\langle\tau\rangle_C = \sigma_\infty\tau_P\langle\tau/\tau_P\rangle_C = \sigma_\infty\tau_P\gamma_{DC}. \tag{A.6}$$

[2] On p 640, next to bottom line, replace $\rho_0\varepsilon_{D\infty}$ by $\rho_0\varepsilon_V\varepsilon_{D\infty}$. The word 'imaginary' on the third line of p 643 should be replaced by 'real'.

Similarly, for the DebD model, equation (A.2) leads to

$$\varepsilon_V \varepsilon_0^2 = \sigma_\infty \tau_D (\varepsilon_0 - \varepsilon_\infty), \tag{A.7}$$

appreciably different from the Deb one of equation (A.6) when $\gamma_{DC} = 1$. In addition, a series constant-phase-element, denoted SC, whose expression at the complex conductivity level is $\sigma_{SC} \equiv \varepsilon_V A_{SC} (i\omega)^{\gamma_{SC}}$, is often found useful with $0 < \gamma_{SC} < 2$.

Let us designate the Davidson–Cole conductive-system model as the DC0. Because its $\varepsilon'(\omega)$ high-frequency limit is zero, when this model is used to fit a given data set it is necessary to include a free parameter representing ε_∞ in parallel, then designated the CDC0 composite model. Although the original derivations of both the DCD and DC0 models were somewhat empirical, it has been shown that the DCD $I_k(\omega)$ model may be derived from fractal considerations [53], as is also likely for the DC0 one [18]. Note that for either DC model, $\langle \tau \rangle_j = \gamma_{DCj} \tau_{DCj}$, where $j =$ D or 0.

A.3. Continuum diffusion models: PNP and PNPA for full dissociation

It is most useful to define these composite models as made up of a normalized interface part involving ordinary or anomalous diffusion, $Z_{iN} \equiv Z_i / R_\infty$, and parts defining the non-anomalous high-frequency limiting behavior of a material containing mobile charges, usually ions, between two plane-parallel blocking electrodes situated a distance L apart. See the discussion on [4, p 1616] for justification of this separation. Here we are primarily concerned with models for charges of both signs mobile with equal mobilities: the usual two-mobile assumption.

Although the present models are derived from microscopic considerations [1, 4, 25] and involve complete blocking at the electrodes, they do not invoke specific hopping and trapping processes but only require that mobile charge can diffuse through the medium, taken as an isotropic continuum. Although this situation seems most appropriate for liquids, the PNPA model has also been successfully applied for analyzing frequency response data for solids of various kinds [54]. The PNP model considers the ions as point-like charges in thermodynamic equilibrium inside a non-dispersive dielectric background representing the polar solvent. It is, therefore, of effective-medium character but neglects possible non-electrostatic steric interactions that become stronger as the concentration of ions increases.

The full result is designated the PNPA model, includes the PNP as a limit, and is defined by the total normalized impedance $Z_{TN} \equiv Z_T / R_\infty$, where Z_T and R_∞ are often expressed for unit electrode area. For full dissociation the relevant parameters of the PNPA are $R_\infty \equiv 1/\sigma_\infty$, C_∞ (or τ_P), M, and ψ, and for specific data R_∞ and C_∞ are replaced by ρ_∞ and ε_∞. Note that the symbol R_∞ is inappropriate because for the PNP model without GR $R_\infty = R'(0)$ but not $R'(\infty)$, which is zero. We nevertheless use R_∞ rather than R_0 here because $R_\infty \equiv 1/G_\infty$ appears in all previous PNP-related work of the author (e.g., [1, 2, 4]), but $\sigma_\infty \equiv \sigma'(\infty)$ is the consistently named quantity. In the present work, ρ_0 may be used, however, for non-blocking models where it is defined as $\rho_0 \equiv \rho'(0)$ and $\rho'(\infty)$ may or may not be negligible.

Here $M \equiv L/2L_D$ is the number of Debye lengths, L_D, in half the electrode separation distance. The range of the PNPA exponent ψ is $0 < \psi \leqslant 1$, with usual PNP response for $\psi = 1$ and PNPA anomalous diffusion for $\psi < 1$. A characteristic relaxation time of these models is $\tau_P \equiv R_\infty C_\infty = \varepsilon_V \varepsilon_\infty / \sigma_\infty$ s. It is thus the conductive-system Debye or Maxwell relaxation time, τ_D, and it may also be expressed as L_D^2/D, where D is the diffusion coefficient. This result may be compared to L^2/D, appropriate for bulk diffusion alone [11].

Since $\varepsilon_V \varepsilon_\infty = \sigma_\infty \tau_P$ for PNPA and PNP models, when the response is thermally activated and ε_∞ is inversely proportional to the absolute temperature, T, it is clear that $T\sigma_\infty$ and τ_P can have the same thermal activation energy, as usually observed. It follows from the above definitions that

$$D = (L/2M)^2 / \tau_P, \tag{A.8}$$

and

$$L_D = (\tau_P / D)^{1/2} = L/2M, \tag{A.9}$$

quantities that can be calculated directly from fitting parameter estimates when L is known. In the two-mobile uni-univalent situation with equal concentrations of positive and negative mobile charge, the Debye length is conventionally expressed as $[\varepsilon_V \varepsilon_\infty k_B T / (2n_0 e^2)]^{1/2}$, where k_B is Boltzmann's constant; e is the charge of equally mobile positive and negative ions; and n_0 is here the mobile charge concentration of the negative charges, a quantity that may also be calculated from an estimate of ρ_∞. For the one-mobile situation, the 2 in the Debye length expression is replaced by 1, and it follows that $L_{D1} = \sqrt{2} L_{D2}$.

Let $\Omega \equiv \omega \tau_P$, then the normalized total impedance, Z_{TN}, of the PNPA model, involving the normalized interface impedance, Z_{iN}, is just

$$Z_{TN} = [1 + Z_{iN}] / [1 + i\Omega (1 + Z_{iN})], \tag{A.10}$$

or in un-normalized terms, Z_T is the series combination of R_∞ and Z_i, all in parallel with C_∞. In the LEVM computer program for fitting PNP and PNPA models to specific data in the absence of GR effects (see the LEVM Manual pp 4–9 and 4–10), a choice between using either τ_P or ε_∞ as a free fitting parameter is included because the latter value leads to less inter-correlations of the parameters and thus usually to a slightly better fit. Note that, as physically required, neither R_∞ nor C_∞ depends on the value of ψ, and from the Nernst–Einstein relation σ_∞ is proportional to the diffusion constant D. But since at very high frequencies charge motion is purely vibratory, this D may be different from that in the bulk at low frequencies where hopping and trapping processes may dominate for some materials. Here, however, we use the same D for the full frequency range of interest.

The completely blocking PNP and PNPA expressions given here apply, for the two-mobile case without GR effects, to a material with both positive and negative charges mobile and with equal mobilities and valences. It has been shown that they also apply when the appropriate Debye length, L_D, is used in the one-mobile, completely blocking, fully dissociated

situation where charge of only a single sign is mobile, possible for solids [2, 4, 10, 25].

Now define $r \equiv M\mathrm{ctnh}(M)$, where, as usual $M \equiv L/2L_D$. Then for the PNP model the ratio of the low-frequency-limiting capacitance, $C_0 \equiv C'(0)$, to the high-frequency value, C_∞, is just r. As $M \to 0$, $r \to 1$ (no space charge) and $C_0 \to C_\infty$, involving just ε_∞, while as M increases, $r \to M$. Thus, for $M \geqslant 4$, $C_0 \cong \varepsilon_V\varepsilon_\infty(A/2L_D)$, where A is the electrode area, and C_0 is just M times the high-frequency limiting capacitance, C_∞, and thus it is equal to the usual diffuse double-layer interface capacitances of two identical electrodes in series.

The PNP charge-transport model was first derived in [1], but has been both simplified in [2] and given in more general terms in [3, 4, 25]. Some of its consequences were discussed and illustrated in [6] for completely blocking electrode situations. Here we generalize the two equivalent completely blocking PNP expressions for Z_{TN} given in equation (1) of [2] to the PNPA. Related anomalous diffusion generalization was done more than two decades ago for ordinary finite-length Warburg diffusion (no satisfaction of the Poisson equation) [55, LEVM Manual, p 4–9, equation (2)] and later independently justified using fractional calculus [56].

The main PNPA interface component, Z_{iN}, may be expressed as

$$Z_{iN} = p^2/[u^2\{q\mathrm{ctnh}(q) - 1\}], \tag{A.11}$$

where $s^2 \equiv i\Omega \equiv i\omega\tau_P$, $u^2 \equiv s^{2\psi}$, $p^2 \equiv 1 + u^2$, and $q \equiv Mp$. Its $\psi = 1$ PNP expression appears in [2–4]. Note that although Z_{iN} involves anomalous diffusion through u^2 and p^2 when $\psi < 1$, Z_{TN} also includes the non-anomalous s^2 parameter, and, on combining equations (A.10) and (A.11), is given by

$$Z_{TN} \equiv Z_T/R_\infty = \rho/\rho_\infty = [Mps^2 + \tanh(q)]/Mp^3s^2. \tag{A.12}$$

This result is also equivalent to equation (3) on p 4–10 of the LEVM Manual, and three fitting expressions for the PNPA Z_T are available in LEVM, using Circuit O with NELEM = 9. In two of these expressions, s^2 appears as in equation (A.10) but for the third it is replaced by the inappropriate anomalous diffusion choice of u^2. Equation (A.12) is fully equivalent to equation (1) in [2] when $\psi = 1$.

In 1983, Coelho [5] used the results of [1] to derive an expression equivalent to that of (A.12) for $\psi = 1$ but expressed in terms of $\varepsilon/\varepsilon_\infty$, without apparently being aware of the 1971 result in [2]. Transformation of equation (A.12), using the relation $\tau_P = \varepsilon_V\varepsilon_\infty/\sigma_\infty$, leads to

$$\varepsilon/\varepsilon_\infty = 1 + [u^2/s^2] \times [\{Mp\mathrm{ctnh}(Mp) - 1\}]/[u^2Mp\mathrm{ctnh}(Mp) + 1], \tag{A.13}$$

which reduces for $\psi = 1$ to Coelho's expression

$$\varepsilon/\varepsilon_\infty = v^2/[s^2 + (\tanh(Mv)/Mv)], \tag{A.14}$$

where $v^2 \equiv (1 + s^2)$. When one then assumes $M \gg 1$ and makes the approximation that $v = 1$, the result may be written as

$$\varepsilon/\varepsilon_\infty \simeq 1 + (M - 1)/[1 + i\omega(M\tau_P)], \tag{A.15}$$

the ordinary DebD result with $\Delta\varepsilon \equiv (M - 1)\varepsilon_\infty$ and $\tau_{DD} \equiv M\tau_P$. The results of Coelho [5] are clarified in the Appendix of [8].

The useful work of [8], whose authors were apparently still unaware in 2006 of the relevant work of [2, 4, 6], shows how the equation (A.15) DebD approximation of the PNP, applied for one-mobile situations, may be used to obtain approximate estimates of the mobilities, ion concentrations, and diffusion constants of their polymer data. More accurate results might have been obtained using the LEVM fitting program with such a composite model as the PNP · Deb one. Another independent attempt to derive a model to characterize ionic bulk densities and diffusion coefficients in nematic liquid crystals [57] has been recently shown to lead to inappropriate results [58].

In 2005, long after the 1953–1988 work on the PNP, an independent solution of its equations led to an expression for Z_T isomorphic with that in [2] except for different parameterization [7]. The resulting numerical and graphical results did not, lead, however, to full agreement with the earlier work because of the use of non-standard definitions of some quantities such as the real part of $\sigma(\omega)$: $\sigma'(\omega)$. Thus, this work did not show the presence of the high-frequency plateau appearing in the proper σ' function.

A recent publication in 2009 by Lenzi *et al* used fractional derivatives to generalize the PNP to produce an anomalous diffusion model [9] for fully dissociated, no GR, conditions. It is very similar to, but independent of, the present PNPA model, equation (A.12), one which was added to LEVM in early 2009 before the Lenzi work was published. Reference [9] does not refer to the earlier PNP work and considers only some response at the impedance level. The current PNP/PNPA model, based on the work of [4] and instantiated in the LEVM fitting program, applies for any mobility ratio and also includes the possibility of invoking anomalous diffusion, as demonstrated in the results of figure 4(a).

References

[1] Macdonald J R 1953 *Phys. Rev.* **92** 4
[2] Macdonald J R 1971 *J. Electroanal. Chem.* **32** 317
[3] Macdonald J R 1973 *J. Chem. Phys.* **58** 4982
Macdonald J R 1974 *J. Chem. Phys.* **60** 343 (erratum)
[4] Macdonald J R and Franceschetti D R 1978 *J. Chem. Phys.* **68** 1614 (See also pp. 4–9 and 4–10 of the LEVMW manual for discussion of a PNPA model available in the LEVMW fitting program)
[5] Coelho R 1983 *Rev. Phys. Appl.* **18** 137
Coelho R 1991 *J. Non-Cryst. Solids* **131** 1136
[6] Macdonald J R 1988 *J. Electrochem. Soc.* **135** 2274 (Below equation (A.1), in γ_j replace θ_j^2 by θ_j, and on p 2279 in t_1 replace ψ by $\psi^{1/2}$)
[7] Barbero G and Alexe-Ionescu A L 2005 *Liquid Cryst.* **32** 943
[8] Klein R J, Zhang S, Dou S and Jones B H 2006 *J. Chem. Phys.* **124** 144903
[9] Lenzi E K, Evangelista L R and Barbero G 2009 *J. Phys. Chem.* B **113** 11371
[10] Derfel G, Lenzi E K, Yednak C R and Barbero G 2010 *J. Chem. Phys.* **132** 224901
[11] Bazant M Z, Thornton K and Ajdari A 2004 *Phys. Rev.* E **70** 021506
[12] Macdonald J R and Potter L D Jr 1987 *Solid State Ion.* **23** 61

Macdonald J R 2000 *J. Comput. Phys.* **157** 280
[13] Scher H and Lax M 1973 *Phys. Rev.* B **7** 4491
[14] Moynihan C T, Boesch L P and Laberge N L 1973 *Phys. Chem. Glasses* **14** 122
[15] Grassberger P and Procaccia I 1982 *J. Chem. Phys.* **77** 6281
[16] Macdonald J R 2009 *J. Phys. Chem.* B **113** 9175
[17] Macdonald J R 2010 *J. Appl. Phys.* **107** 101101
[18] Davidson D W and Cole R H 1951 *J. Chem. Phys.* **19** 1417
Davidson D W 1961 *Can. J. Chem.* **39** 571
[19] Macdonald J R 1997 *J. Non-Cryst. Solids* **212** 95 (The symbol 'sigma' should be removed from the right end of equation (12))
[20] Macdonald J R 2002 *J. Chem. Phys.* **116** 3401
[21] Macdonald J R 2002 *Solid State Ion.* **150** 263 (The symbol $\rho_{C1\infty}$ at the left side of the equation above figure 6 on p 274 should be replaced by $\tau_{C1\infty}$)
[22] Macdonald J R 2004 *J. Appl. Phys.* **95** 1849
[23] Macdonald J R 2005 *Phys. Rev.* B **71** 184307
[24] Macdonald J R 2009 *J. Phys. Chem. Solids* **70** 546 (The data here were incorrectly treated as specific in character)
[25] Macdonald J R, Franceschetti D R and Meaudre R 1977 *J. Phys. C: Solid State Phys.* **10** 1459
[26] Barbero G and Lelidis I 2010 *J. Phys. Chem.* B submitted
[27] Alexe-Ionescu A L 2010 private communication
[28] Serghei A, Tress M, Sangoro J R and Kremer F 2009 *Phys. Rev.* B **80** 184301
[29] Lunkenheimer P, Fichtl R, Ebbinghaus S G and Loidl A 2004 *Phys. Rev.* B **70** 172102
[30] Krohns S, Lunkenheimer P and Ebbinghaus S G 2007 *Appl. Phys. Lett.* **91** 022910
[31] Lunkenheimer P, Krohns S, Riegg S, Ebbinghaus S G, Reller A and Loidl A 2010 *Eur. Phys. J. Spec. Top.* **180** 61
[32] Lunkenheimer P 2010 private communication
[33] Macdonald J R 1999 *Braz. J. Phys.* **29** 332
[34] Macdonald J R 2005 *J. Phys.: Condens. Matter* **17** 4369
[35] Pajkossy T 1997 *Solid State Ion.* **94** 123
[36] Macdonald J R and Ahmad M M 2007 *J. Phys.: Condens. Matter* **19** 046215
[37] Lindsay G P and Patterson G D 1980 *J. Chem. Phys.* **73** 3348
[38] Larsen A E, Grier D G and Halsey T C 1995 *Phys. Rev.* E **52** R2161
[39] Kerner Z and Pajkossy T 2000 *Electrochim. Acta* **46** 207
[40] Kilic M S, Bazant M Z and Ajdari A 2007 *Phys. Rev.* E **75** 021502
[41] Macdonald J R and Barlow C A Jr 1962 *J. Chem. Phys.* **36** 3062
[42] Macdonald J R 1981 *Mol. Phys.* **44** 1043
[43] Macdonald J R, Lehnen A P and Franceschetti D R 1982 *J. Phys. Chem. Solids* **43** 39
[44] Macdonald J R and Kenkel S W 1984 *J. Chem. Phys.* **81** 3215
[45] Macdonald J R 1987 *J. Electroanal. Chem.* **223** 1
[46] Macdonald J R 1992 *J. Phys. Chem.* **96** 3861
[47] Macdonald J R 1992 *Phys. Rev.* A **46** R2988
[48] Bazant M Z, Kilic M S, Storey B D and Ajdari A 2009 *Adv. Colloid Interface Sci.* **152** 48
[49] Hamou R F, Biedermann P U, Erbe A and Rohwerder M 2010 *Electrochim. Acta* **55** 5210
[50] Cagle C, Feng G, Qiao R, Huang J, Sumpter B G and Meunier V 2010 *Microfluid Nanofluid* **8** 703
[51] Macdonald J R 2006 *J. Phys.: Condens. Matter* **18** 629
[52] Macdonald J R 2000 *Solid State Ion.* **133** 79
[53] Nigmatullin R R and Ryabov Ya E 1997 *Phys. Solid State* **39** 87
[54] Macdonald J R 2010 unpublished work
[55] Macdonald J R 1985 *J. Appl. Phys.* **58** 1955
[56] Bisquert J and Compte A 2001 *J. Electroanal. Chem.* **499** 112
[57] Sawada A, Nakazono Y, Tarumi K and Naemura S 1998 *Mol. Cryst. Liq. Cryst. Sci. Technol.* A **318** 225
[58] Alexe-Ionescu A L, Barbero G and Lelidis I 2009 *Phys. Rev.* E **80** 061203